The 7th International Supercritical CO_2 Power Cycles Symposium
February 21-24, 2022, San Antonio, Texas
Paper #38

Defining Temperature Limitations for Steels in sCO_2 Applications

Bruce A. Pint
Group Leader
Oak Ridge National Laboratory
Oak Ridge, TN 37831-6156 USA

Rishi Pillai
R&D Staff Member
Oak Ridge National Laboratory
Oak Ridge, TN 37831-6156 USA

James R. Keiser
Distinguished R&D Staff Member
Oak Ridge National Laboratory
Oak Ridge, TN 37831-6156 USA

ABSTRACT

The current project is evaluating creep-strength enhanced ferritic (CSEF) and austenitic steel performance in supercritical CO_2 (sCO_2) conditions at 450°-650°C to determine the temperature limit for these lower cost materials. The study is evaluating representative 9 and 12%Cr steels and conventional and advanced austenitic steels. Results are shown in 300 bar research grade (RG) sCO_2. As expected, the austenitic steels 316H and 709 showed low mass gains and the CSEF steels showed much higher mass gains after 2,000 h at 450° and 550°C consistent with the formation of a duplex oxide scale and other data in the literature. At 650°C, only the advanced austenitic steel, alloy 709, maintained the formation of a thin Cr-rich oxide scale with no significant C ingress and no loss in room temperature ductility. The other steels formed Fe-rich oxide scales with significant C uptake and loss in ductility after a 1,000 h exposure at 650°C.

INTRODUCTION

A number of power generation technologies are interested in the use of supercritical CO_2 (sCO_2), including nuclear, fossil, geothermal, concentrating solar power (CSP) and waste heat recovery, because of its unique properties and relatively low critical point (31°C/73.8 bar) [e.g. Dostal 2006, Chen 2010, Iverson 2013, Wright 2013, Cheang 2015]. Steels like Grade 9 (Fe-9Cr-1Mo) used in the UK advanced gas cooled reactors (AGR) operated at 43 bar CO_2 (sub-critical) and ≤550°C could be severely internally carburized in those conditions [Gong 2017], so there have been numerous materials studies in sCO_2 to determine the temperature limitations of various classes of materials [Moore 2012, Pint 2017a]. Much of the early work focused on Fe-based alloys [Dunlevy, 2009, Furukawa, 2011, Rouillard 2011, Tan 2011]. More recent studies have confirmed that Ni-based alloys are compatible with sCO_2 at temperatures up to 800°C [Lee 2015, Olivares 2015, 2018, Oleksak 2018, Pint 2020] even in the presence of high impurity levels [Mahaffey 2016, Kung 2016, Pint 2019a]. However, for sCO_2 cycles to be commercially competitive, lower cost steels are needed at lower temperatures. A recent review suggested that creep-strength enhanced ferritic (CSEF) steels were limited to 450°C in sCO_2 [Sarrade 2017], much lower than the 580°-600°C limit in supercritical steam [Shingledecker 2013] and suggesting that surface modifications should be investigated to improve sCO_2 compatibility.

The current project exposed both CSEF and austenitic steels at 450-650°C to determine maximum use temperatures in both direct- and indirect-fired cycles [Allam 2013,Wright 2013]. The overall plan was to expose specimens for at least 1000 h at 300 bar in RG sCO_2 and in RG sCO_2 with

controlled O_2 and H_2O additions [Pint 2019a, 2021, 2022] to simulate the Allam cycle. In addition to mass change and oxide thickness, room temperature ductility and bulk C content were measured to assess compatibility. A subset of RG sCO_2 results from this project are presented.

EXPERIMENTAL PROCEDURE

The chemical compositions of the structural steels studied are shown in Table 1. Alloy coupons (~12 x 20 x 1.5mm) were polished to a 600 grit finish. The tensile specimens were 25 mm long (designated SS-3) with a gage of 0.8 x 5 mm, a surface area of ~1.9 cm^2, and a 600 grit machined finish. All specimens were ultrasonically cleaned in acetone and methanol prior to exposure. The specimens were exposed for 500-h cycles at 550°C in 300 bar RG sCO_2. The exposures were conducted in a vertically-oriented autoclave (~266 mm x 83 mm inner diameter) made from Ni-based alloy 282 and operated inside a three-zone furnace with an alloy 282 sample rack that sat on the bottom of the autoclave. The fluid flow rate was ~2 ml/min and additional details of the system have been provided elsewhere [Pint 2015,2017b]. The specimens were slowly heated to temperature over several hours (~2°C/min) in sCO_2, held at temperature ±2°C and then cooled in CO_2 to room temperature. Previously, the H_2O content of the RG CO_2 was measured by the vendor in 6 cylinders as 4.1±0.7 ppm.

Because of variability observed in previous experiments, 6 coupons and 4 SS-3 specimens were included of each alloy. Before and after exposure, all specimens were weighed using a Mettler Toledo model XP205 balance with an accuracy of ~±0.04 mg or 0.01 mg/cm^2. For characterization, specimens were copper plated before being sectioned and mounted for light microscopy. Room temperature tensile tests used a strain rate of 0.015/min per ASTM E8-13. Bulk C content was measured using combustion analysis. Additional characterization is presented elsewhere [Pint 2021,2022].

RESULTS AND DISCUSSION

As an example of the data collected, Figure 1 shows the mass change data obtained during 500-h cycles at 550°C using two similar groups of specimens. The boxes show the 25% and 75% values of the 5-6 polished coupons exposed of each alloy, the whiskers show the minimum and maximum values measured and the median values are shown for each group. As expected, the 9-12%Cr steels showed much higher mass gains than the austenitic steels. The increased Cr

Table 1. Chemical composition of the alloys measured by inductively coupled plasma and combustion analyses in mass%.

Alloy	Fe	Cr	Ni	Mo	Mn	Si	C	Other
T91	88.8	8.6	0.3	0.9	0.46	0.35	0.099	0.2V,0.1Nb,0.045N
VM12	83.3	11.5	0.4	0.4	0.38	0.42	0.120	1.5Co,1.6W,0.2V,0.036N
316H	69.5	16.3	10.0	2.0	0.84	0.46	0.040	0.08V,0.039N,0.02Nb
304H	70.0	18.3	8.6	0.3	1.8	0.31	0.073	0.07V,0.4Cu,0.2Co,0.064N
347H	69.2	17.1	10.2	0.4	1.7	0.29	0.034	0.6Nb,0.1Co,0.2Cu,0.022N
709	51.3	20.1	25.2	1.5	0.89	0.41	0.064	0.2Nb,0.15N
Sanicro 25	42.6	22.3	25.4	0.2	0.52	0.15	0.068	3.5W,1.5Co,3.0Cu,0.21N
310HCbN	51.0	25.7	20.4	0.07	1.2	0.36	0.065	0.5Nb,0.3Co,0.25N

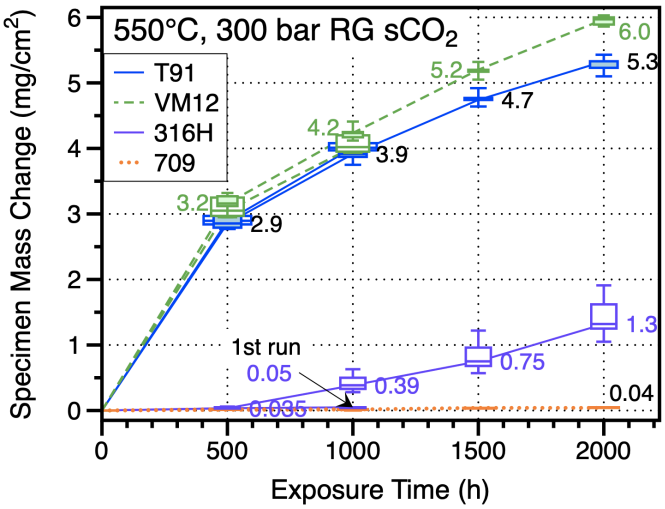

Figure 1. Specimen mass gain during 500-h cycles at 550°C in 300 bar RG sCO_2. Box and whisker plots show data for 5-6 specimens exposed and the median values are shown.

content in VM12 did not reduce the reaction rate at this temperature. Both sets of specimens showed similar mass gains after 1000 h. Both austenitic steels showed very low mass gains during exposure of the first set of specimens stopped after 1,000 h. For the second set of specimens, the alloy 709 specimens showed low mass gains after 2,000 h, but the 316H specimens showed much higher mass gains. Similar experiments were conducted at 450°C (2,000 h) and 650°C (1,000 h).

Assuming parabolic kinetics from Figure 1, Figure 2 shows calculated rates compared to literature values [Pint 2017a]. The rates for T91 and VM12 were very similar to those reported previously

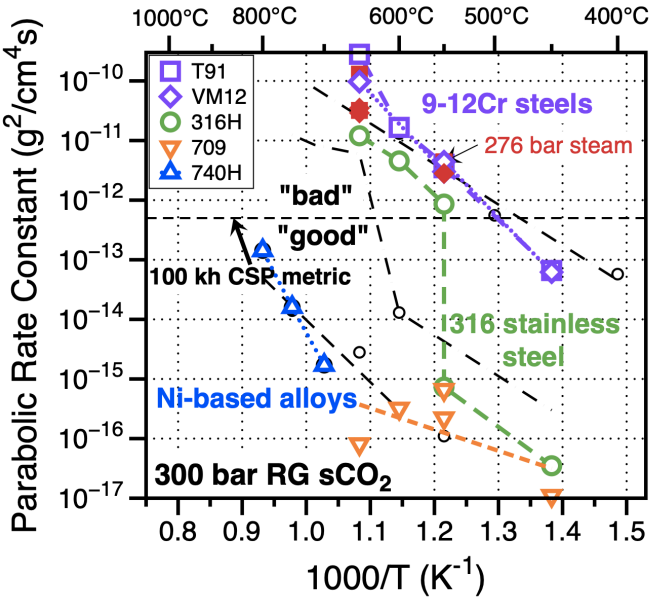

Figure 2. Arrhenius plot of literature parabolic rate constants and estimated rates from this study.

in sCO_2 [e.g. Furukawa 2011] and in high pressure steam [Pint 2019b], Figure 2. The rates for alloy 709 were very low and difficult to measure but consistent with Ni-based alloys, like 740H. Rates for 316H transitioned between low rates at 450°-550°C when Cr-rich oxides formed and higher rates at higher temperatures where Fe-rich oxides formed.

Figure 3 shows example light microscopy of specimens of each alloy exposed at each temperature for 1,000 h. Similar to previous observations in 200 bar RG sCO_2 [Pint 2016], the CSEF steels formed a duplex microstructure with an outward growing magnetite (Fe_3O_4) outer layer and in inward growing, $(Fe,Cr)_3O_4$ inner layer [e.g. Furukawa, 2011, Rouillard 2011, Tan 2011]. The low mass gains for the austenitic steel specimens are associated with very thin Cr-rich oxides at 450° and 550°C. However, at 650°C, the alloy 709 specimens continued to form a thin oxide while the 316H specimens formed Fe-rich oxides (the outer layer spalled after 1,000 h in Figure 3).

The project test matrix is straight forward and has generated reaction rates, rate constants, activation energies and representative oxide thickness values. However, it is not clear that rate constants are really the key metric for this application. A CSP-related project [Pint 2020] had a metric of the parabolic rate constant being less than 5×10^{-13} g^2/cm^4s, Figure 2. To move beyond the reaction kinetics, small SS-3 type tensile specimens of several alloys were previously exposed at 750°C in sCO_2 [Pint 2019a, Dryepondt 2022]. A dramatic drop in ductility (i.e. total elongation) was observed for the 304H specimens in CO_2 and sCO_2 after ≤ 1,000 h exposures that was not observed after similar exposures in laboratory air.

For this project, one SS-3 specimen of each alloy was removed after each cycle at each temperature and a few of the room temperature tensile results are shown in Figure 4 with a comparison to the as-received and Ar-annealed properties for each alloy. After these 1,000 h exposures, there was little change in properties at 550°C. The annealing was performed to isolate the sCO_2 effect from any effects of the thermal treatment. There was some drop in the 0.2% yield

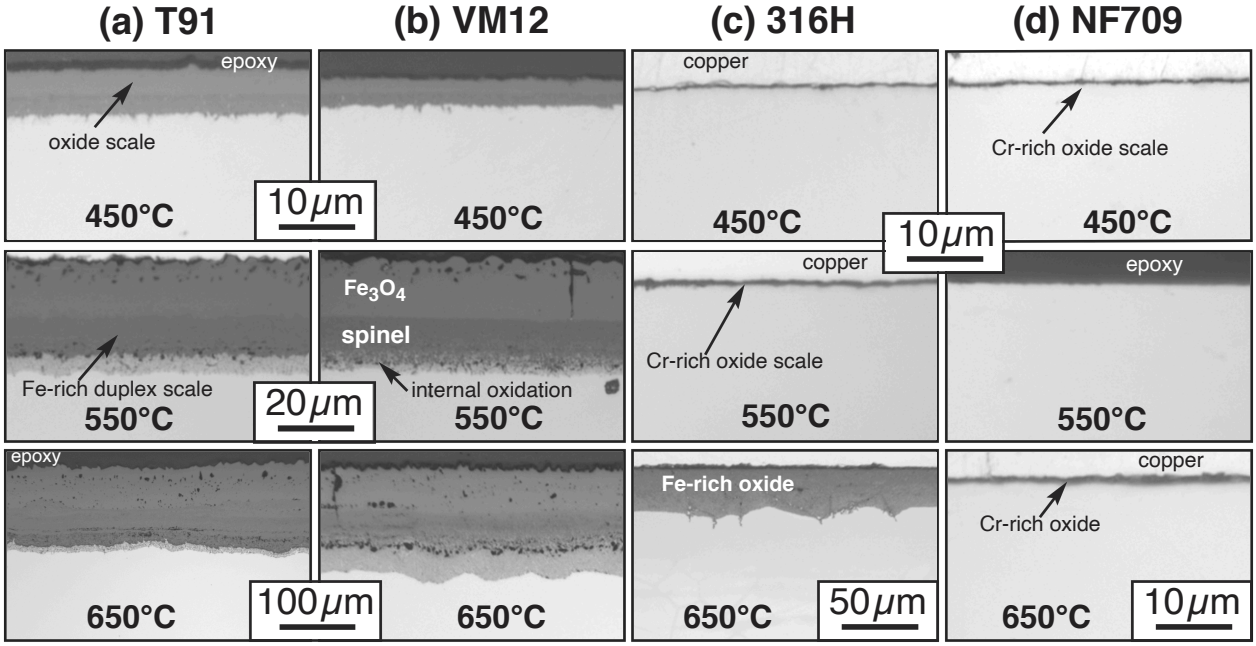

Figure 3: Light microscopy of polished cross-sections of specimens exposed for 1,000 h at three different temperatures in 300 bar RG CO_2.

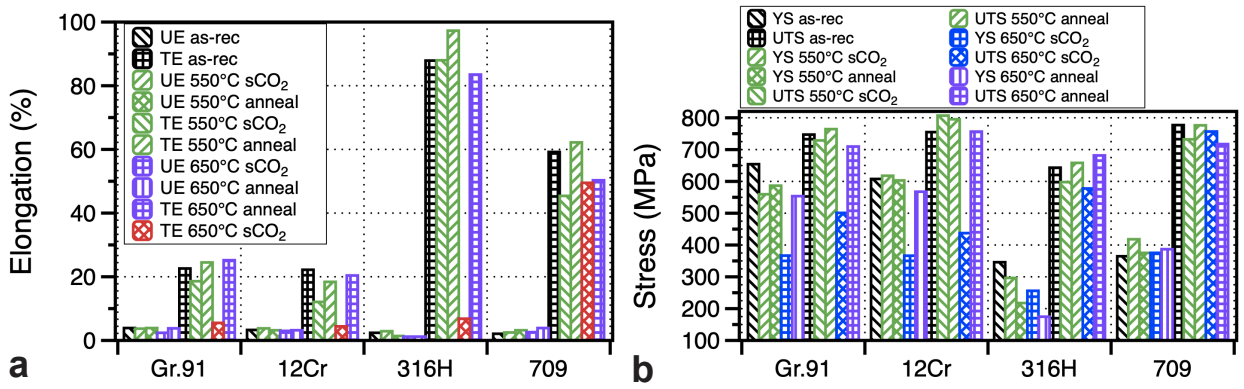

Figure 4. Comparison of 22°C tensile properties before and after 1,000 h exposures at 550°C and 650°C in RG sCO_2 or Ar (a) uniform and total elongation and (b) yield and ultimate tensile strength.

strength for 316H after 1000 h at 550°C, Figure 4b. After similar exposures at 650°C, there was a large drop in total elongation for the steels that formed Fe-rich oxides, highlighted in Figure 4a. No drop was observed for the alloy 709 specimen that formed a Cr-rich oxide. In Figure 4b, the 650°C sCO_2 exposure also appeared to impact the CSEF strength values.

This embrittlement has been observed previously and attributed to C uptake in 1 bar CO_2 [McCoy 1965, Martin 1965]. The oxygen potential gradient across the scale creates an opposite chemical potential gradient driving C diffusion inward [Gheno 2011] perhaps via defects in rapidly growing Fe-rich oxide scales. While many recent studies have looked for a C-rich layer beneath the oxide scale, earlier studies used bulk C measurements to quantify the ingress [McCoy 1965, Martin 1965]. Figure 5a confirms that the C content was increased in the alloys showing degradation at 650°C and that no bulk C content was detected at lower temperatures. Figure 5b shows C content data for several austenitic steels exposed at 750°C in 300 bar RG or IG sCO_2. The previously mentioned embrittlement of type 304SS at 750°C can be attributed to C uptake. Both at 650°C (alloy 709 for 1,000 h) and at 750°C (alloys Sanicro 25 and 310HCbN or HR3C for 10 kh), these advanced austenitic steels with higher Cr and Ni contents (Table 1) formed thin, protective Cr-rich

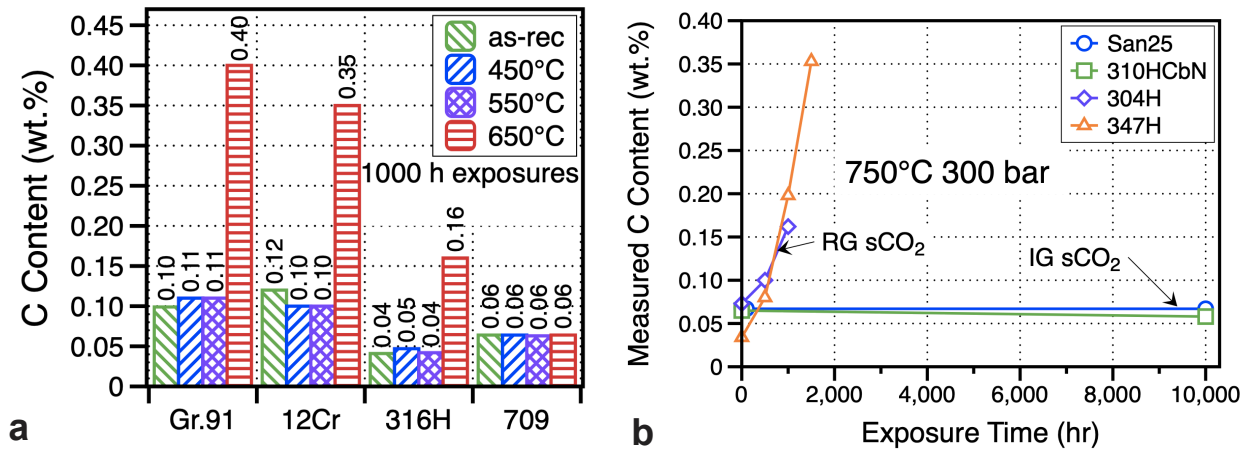

Figure 5. Measured C content after exposures in 300bar RG or IG sCO_2 (a) as-received and after 1,000h exposures at 450°-650°C and (b) as a function of exposure time at 750°C.

oxide scales in sCO_2 that appears to prevent C ingress in these conditions. In contrast, the conventional austenitic steel specimens showed high C uptake after 500-1500 h exposures in RG sCO_2 at 650° and 750°C, Figures 5a and 5b. The ultimate goal of this project will be to model C uptake as a function of exposure temperature, similar to the work performed for the 43 bar AGR application where the gas C activity is intentionally higher [Gong 2017]. Measurements of C profiles from these specimens [Pint 2022] will help to validate the model. The model will help to identify temperature ranges where these materials can be safely used in sCO_2 applications.

The final stage of this project will be to evaluate the performance of various surface modifications (e.g. Cr and Al-rich coatings, shot peening) to determine if sCO_2 compatibility can be improved to further expand deployment (particularly for the CSEF steels).

CONCLUSIONS

A subset of results were reported for four candidate steels for application in supercritical CO_2 applications. After exposures at 450°-650°C in 300 bar (30 MPa) RG sCO_2, the CSEF steel specimens, T91 and VM12, showed much higher mass gains than the austenitic steel specimens, 316H and 709 at 450° and 550°C, with rates similar to those previously reported. Only alloy 709 specimens formed a thin protective scale at 650°C. Moving beyond mass change data and reaction product characterization, post-exposure room temperature tensile testing of these alloys showed minor changes after 550°C exposures but more substantial losses in ductility after 650°C exposures where an Fe-rich oxide was formed. The drop in ductility was correlated to an increase in bulk C content, similar to prior observations. Advanced austenitic steels like alloy 709 appeared to resist C uptake and room temperature embrittlement by forming a protective Cr-rich oxide scale.

NOMENCLATURE

CSP	=	Concentrating Solar Power
CSEF	=	Creep strength enhanced ferritic
IG	=	Industrial Grade
ORNL	=	Oak Ridge National Laboratory
RG	=	Research Grade
UK	=	United Kingdom

REFERENCES

Allam, R. J., Palmer, M. R., Brown Jr., G. W., Fetvedt, J., Freed, D., Nomoto, H., Itoh, M., Okita, N., Jones Jr., C., 2013, “High efficiency and low cost of electricity generation from fossil fuels while eliminating atmospheric emissions, including carbon dioxide,” Energy Procedia 37, 1135–1149.

Cheang, V., Hedderwick, R. A, McGregor, C., 2015, “Benchmarking supercritical carbon dioxide cycles against steam Rankine cycles for Concentrated Solar Power,” Solar Energy, 113, 199-211.

Chen, H., Goswami, D. Y., Stefanakos, E. K., 2010, “A review of thermodynamic cycles and working fluids for the conversion of low-grade heat,” Renewable & Sustainable Energy Reviews 14, 3059-3067.

Dostal, V., Hejzlar, P., Driscoll, M. J., 2006, “The supercritical carbon dioxide power cycle: Comparison to other advanced power cycles,” Nuclear Technology, 154(3), 283-301.

Dryepondt, S., Lehmusto, J., Pint, B. A., 2022, “Effect of Annealing and Supercritical CO_2 Exposure at 750 °C on the Tensile Properties of Stainless Steel and Ni-based Structural Alloys,” Materials

and Corrosion, in press.

Dunlevy, M. W., 2009, “An Exploration of the Effect of Temperature on Different Alloys in Supercritical Carbon Dioxide Environment,” M.Sc. Thesis, MIT, Cambridge, MA.

Furukawa, T., Inagaki, Y., Aritomi, M., 2011, “Compatibility of FBR structural materials with supercritical carbon dioxide,” Progress in Nuclear Energy 53, 1050–1055.

Gheno, T., Monceau, D., Zhang, J., Young, D. J., 2011 “Carburisation of Ferritic Fe-Cr Alloys by Low Carbon Activity Gases,” Corrosion Science 53, 2767-2777.

Gong, Y., Young, D. J., Kontis, P. Chiu, Y. L., Larsson, H., Shin, A., Pearson, J. M., Moody, M. P., Reed, R. C., 2017, “On the breakaway oxidation of Fe9Cr1Mo steel in high pressure CO_2,” Acta Materialia, 130, 361-374.

Iverson, B. D., Conboy, T. M., Pasch, J. J., Kruizenga, A. M., 2013, “Supercritical CO_2 Brayton cycles for solar-thermal energy,” Applied Energy, 111, 957-970.

Kung, S. C., Shingledecker, J. P., Thimsen, D., Wright, I. G., Tossey, B. M., Sabau, A. S., 2016, “Oxidation/Corrosion in Materials for Supercritical CO_2 Power Cycles,”in Proceedings of the 5th International Symposium on Supercritical CO_2 Power Cycles, San Antonio, TX, Paper #9.

Lee, H. J., Kim, H., Kim, S. H., Jang, C., 2015, “Corrosion and carburization behavior of chromia-forming heat resistant alloys in a high-temperature supercritical-carbon dioxide environment,” Corrosion Science 99 (2015) 227–239.

Mahaffey, J., Adam, D., Brittan, A., Anderson, M., Sridharan, K., 2016, “Corrosion of Alloy Haynes 230 in High Temperature Supercritical Carbon Dioxide with Oxygen Impurity Additions,” Oxidation of Metals 86, 567-580.

Martin, W. R., Weir, J. R., 1965, “Influence of Chromium Content on Carburization of Chromium-Nickel-Iron Alloys in Carbon Dioxide,” Journal of Nuclear Materials 16, 19-24.

McCoy, H. E., 1965, “Type 304 Stainless Steel vs Flowing CO2 at Atmospheric Pressure and 1100-1800°F,” Corros., 21, 84-94.

Moore, R., Conboy, T., 2012, “Metal Corrosion in a Supercritical Carbon Dioxide – Liquid Sodium Power Cycle,” Sandia National Laboratory Report SAND2012-0184.

Oleksak, R. P., Tylczak, J. H., Carney, C. S., Holcomb, G. R., Dogan, O. N., 2018, “High-Temperature Oxidation of Commercial Alloys in Supercritical CO_2 and Related Power Cycle Environments,” JOM 70, 1527-1534.

Olivares, R. I., Young, D. J., Marvig, P., Stein, W., 2015, “Alloys SS316 and Hastelloy-C276 in Supercritical CO_2 at High Temperature,” Oxid. Met. 84, 585–606.

Olivares, R. I., Young, D. J., Nguyen, T. D., Marvig, P., 2018, “Resistance of High-Nickel, Heat-Resisting Alloys to Air and to Supercritical CO2 at High Temperatures,” Oxid. Met. 90, 1-25.

Pint B. A., Keiser, J. R., 2015, “Initial Assessment of Ni-Base Alloy Performance in 0.1 MPa and Supercritical CO_2,” JOM 67(11), 2615-2620.

Pint B. A., Brese, R. G., Keiser, J. R., 2016, “Supercritical CO_2 Compatibility of Structural Alloys at 400°-750°C,” NACE Paper C2016-7747, Houston, TX, presented at NACE Corrosion 2016, Vancouver, Canada, March 2016.

Pint B. A., Brese, R. G., 2017, “High-Temperature Materials,” in Fundamentals and Applications of Supercritical Carbon Dioxide Based Power Cycles, K. Brun and P. Friedman, eds., Elsevier,

London, pp.67-104.

Pint, B. A., Unocic, K. A., 2018, “The Effect of CO_2 Pressure on Chromia Scale Microstructure at 750°C,” JOM 70, 1511-1519.

Pint, B. A., Lehmusto, J., Lance M. J., Keiser, J. R., 2019a, “The Effect of Pressure and Impurities on Oxidation in Supercritical CO_2,” Materials and Corrosion, 70, 1400-1409.

Pint, B. A., Pearson, S. R., De Las Casas Aranda, R., Lance, M. J., Raiman, S. S., Kung, S. C., 2019b, “Water Chemistry and Pressure Effects on Steam Oxidation of Ferritic and Austenitic Steels,” in Proceedings of the Joint EPRI – 123HiMAT International Conference on Advances in High Temperature Materials, J. Shingledecker and M. Takeyama eds., ASM International, Materials Park, OH, pp.939-947.

Pint, B. A., Pillai, R., Lance M. J., Keiser, J. R., 2020, “Effect of Pressure and Thermal Cycling on Long-Term Oxidation in CO_2 and Supercritical CO_2” Oxidation of Metals 94, 505–526.

Pint, B. A., Pillai, R., Keiser, J. R., 2021 “Effect of Supercritical CO_2 on Steel Ductility at 450°-650°C” ASME Paper #GT2021-59383, for Turbo Expo 2021 Virtual Conference and Exhibition, June 11-15, 2021.

Pint, B. A., Lance M. J., Pillai, R., Keiser, J. R., 2022 “Compatibility of Steels at 450°-650°C in Supercritical CO_2 with O_2 and H_2O Additions” NACE Paper C2022-18018, Houston, TX, presented at Corrosion 2022, San Antonio, TX.

Rouillard, F., Charton, F., Moine, G., 2011 “Corrosion Behavior of Different Metallic Materials in Supercritical Carbon Dioxide at 550°C and 250 bars,” Corrosion 67(9), 095001

Sarrade, S., Férona, D., Rouillard, F., Perrin, S., Robin, R., Ruiz, J.-C., Turc, H.-A., 2017, “Overview on corrosion in supercritical fluids,” J. of Supercritical Fluids 120 (2017) 335–344.

Shingledecker, J. P., Pint, B. A., Sabau, A. S., Fry, A. T., Wright, I. G., 2013, “Managing Steam-Side Oxidation and Exfoliation in USC Boiler Tubes,” Advanced Materials and Processing, 171 (1), 23-25.

Tan, L. Anderson, M., Taylor, D., Allen, T. R., 2011, “Corrosion of austenitic and ferritic-martensitic steels exposed to supercritical carbon dioxide,” Corrosion Science 53, 3273-3280.

Wright, I. G., Pint, B. A., Shingledecker, J. P., Thimsen, D., 2013, “Materials Considerations for Supercritical CO_2 Turbine Cycles,” ASME Paper #GT2013-94941, presented at the International Gas Turbine & Aeroengine Congress & Exhibition, San Antonio, TX, June, 3-7, 2013.

ACKNOWLEDGMENTS

The authors would like to thank M. Howell, B. Johnston, T. M. Lowe, T. Jordan and V. Cox for assistance with the experimental work. D. Sulejmanovic and M. J. Lance provided helpful comments on the manuscript. This research was sponsored by the U.S. Department of Energy, Office of Fossil Energy, Crosscutting Technology Program. This manuscript has been authored by UT-Battelle, LLC under Contract No. DE-AC05-00OR22725 with the U.S. Department of Energy. The United States Government retains and the publisher, by accepting the article for publication, acknowledges that the United States Government retains a non-exclusive, paid-up, irrevocable, world-wide license to publish or reproduce the published form of this manuscript, or allow others to do so, for United States Government purposes. The Department of Energy will provide public access to these results of federally sponsored research in accordance with the DOE Public Access Plan (http://energy.gov/downloads/doe-public-access-plan).